Journal of Power Sources 258 (2014) 210–217

Contents lists available at ScienceDirect

Journal of Power Sources

journal homepage: www.elsevier.com/locate/jpowsour

Capacity fade of $LiAl_yNi_{1-x-y}Co_xO_2$ cathode for lithium-ion batteries during accelerated calendar and cycle life tests (surface analysis of $LiAl_yNi_{1-x-y}Co_xO_2$ cathode after cycle tests in restricted depth of discharge ranges)

Shoichiro Watanabe [a,*], Masahiro Kinoshita [b], Takashi Hosokawa [c], Kenichi Morigaki [d], Kensuke Nakura [b]

[a] Portable Rechargeable Battery Business Division, SANYO Electric Co., Ltd., Automotive & Industrial Systems Company of Panasonic Group, 139-32, Toyohisa, Matsushige-Cho, Itano-gun, Tokushima 771-0213, Japan
[b] Device Solution Center, Panasonic Corporation, 1006 Kadoma, Kadoma City, Osaka 571-8501, Japan
[c] Automotive Battery Business Division, SANYO Electric Co., Ltd., Automotive & Industrial Systems Company of Panasonic Group, 194-4, Tokonabe-cho, Kasai City, Hyogo 675-2332, Japan
[d] National Institute of Advanced Industrial Science and Technology (AIST), Research Institute for Ubiquitous Energy Devices, 1-8-31 Midorigaoka, Ikeda, Osaka 563-8577, Japan

HIGHLIGHTS

- We investigated the cycle deterioration of Li-ion cell with NCA cathode.
- Cycle tests with ΔDOD restriction and surface analysis of cathode were carried out.
- NCA cathode material particles are formed by aggregation of primary particles.
- Many microcracks were generated in the inter-surface between the primary particles.
- NiO-like resistance layer with Fm3m structure was formed on each primary particle.

ARTICLE INFO

Article history:
Received 28 October 2013
Received in revised form
31 December 2013
Accepted 6 February 2014
Available online 15 February 2014

Keywords:
Scanning transmission electron energy-loss spectroscopy
Deterioration
Cycle performance
Micro-crack
Lithium nickel cobalt aluminum oxide
Lithium-ion batteries

ABSTRACT

Cycle performance at 60 °C for a Li $Al_{0.10}Ni_{0.76}Co_{0.14}O_2$ (NCA) cathode/graphite cell was greatly improved when a DOD range in charge–discharge cycling (ΔDOD) was restricted. The deterioration mechanism was analyzed by X-ray photoelectron spectroscopy (XPS), high-angle annular dark-field scanning transmission electron microscopy (HAADF-STEM) and scanning transmission electron microscopy-electron energy-loss spectroscopy (STEM-EELS). Only after the cycle test in the ΔDOD of 0–100%, many micro-cracks were generated in the inter-surface between the primary particles which aggregated to form the secondary particles, and a NiO-like resistance layer with Fm3m rock salt structure was formed on each primary particle which was contact with other primary particles and electrolyte. It can be concluded that the lack of contact between the primary particles with the micro-crack generation and the formation of the new resistance layer are responsible for the capacity fading and the rise in impedance during charge–discharge cycle in the wide ΔDOD.

1. Introduction

Lithium-ion batteries (LIBs) with a Li $Al_{0.10}Ni_{0.76}Co_{0.14}O_2$ (NCA) cathode are widely widespread as power supply for notebook PCs and digital still cameras. Moreover, they are also promising as power supply for power storages and battery electric vehicles because of their high capacity and long-term storage characteristics. We have reported that capacity fading depended on ΔDOD, and many micro-cracks, which caused significant discharge capacity loss, were generated in the NCA particles when cycle tests of a cylindrical LIB with the NCA cathode were performed under the conditions of wider ΔDODs and higher temperatures [1,2].

* Corresponding author. Tel.: +81 88 699 9395; fax: +81 88 699 9046.
E-mail address: watanabe.sho-ichiro@jp.panasonic.com (S. Watanabe).

http://dx.doi.org/10.1016/j.jpowsour.2014.02.018
0378-7753/

On the other hand, the deterioration mechanism of the NCA cathode has been clarified by the recent researches with various spectroscopic methods such as X-ray photoelectron spectroscopy (XPS), Fourier transform infrared spectroscopy (FT-IR), attenuated total reflection – Fourier transform infrared spectroscopy (ATR-FTIR), high resolution hard XPS and so on. Abraham et al. found that the deterioration of the NCA cathode mainly contributed to the rise in cell impedance, and the cathode surface film was a mixture of polycarbonates, LiF and Li_xPF_y-type and $Li_xPF_yO_z$-type compounds by XPS [3,4].

Kostecki et al. reported that a thin and non-uniform solid electrolyte interface (SEI) film which was decomposition products of electrolyte such as LiF, Li_xPF_y-type and $Li_xPF_yO_z$-type compounds did not inhibit lithium-ion transport through the interface of cathode/electrolyte, and the loss of electric contacts caused cathode deterioration. They demonstrated electric conductivity of the cathode surface was significantly diminished after a cycle test in the ΔDOD of 0–100% by using current-sensing atomic force microscopy imaging. [5]. Abraham et al. proposed that an oxygen-deficient surface layer was formed on a $LiNiCoO_2$ cathode due to oxygen-transfer reactions with the electrolyte by using X-ray absorption spectroscopy (XAS), the electron energy loss spectroscopy (EELS) and transmission electron microscope (TEM) [6,7]. The cathode surface was turned to a $Li_xNi_{1-x}O$ type (NaCl-type) structure which was believed to contribute to impedance rise of the cathode.

Tatsumi et al. proposed a schematic degradation model of $LiAl_yNi_{1-x-y}Co_xO_2$ by combining spectroscopic methods such as X-ray absorption near-edge structure (XANES), X-ray photoemission spectroscopic (PES) and high-resolution hard X-ray photoemission spectroscopy (HX-PES) [8–10]. In their deterioration model of NCA, the $Li_xAl_{0.10}Ni_{0.73}Co_{0.17}O_2$ surface was a multilayer of Li deficient cubic phase layer and surface films which were composed of Li_2CO_3, hydrocarbons, $ROCO_2Li$, polycarbonate-type compounds, P–O containing compounds and LiF.

Zheng et al. used STEM and EELS to clarify that the extended grain boundary layers were formed and increased during the first charge–discharge cycle [11,12]. The structure of grain boundary was continuously changed from interior to the surface, from the layered structure to a disordered rock-salt structure via a partially ordered structure. They suggested that the microstructure change was primarily responsible for the irreversible capacity at the first cycle. We reported that a cylindrical battery with the NCA cathode exhibited excellent long-term storage and cycling characteristics without increasing the grain boundary in the restricted ΔDOD conditions [2]. In this study, deterioration mechanism of LIBs with the NCA cathode during charge–discharge cycle tests in restricted ΔDODs was investigated by XPS, STEM, and TEM-EELS.

2. Experimental

2.1. Cycle tests in restricted ΔDODs for cylindrical model cells

The cylindrical model cells with capacity of 400 mAh were used. These cells were composed of the NCA cathode which consisted of NCA, DENKA black, and polyvinylidene fluoride, the graphite anode which consisted of graphite and styrene-butadiene rubber, electrolyte and micro-porous polyethylene separator. Electrolyte was a mixture of ethylene carbonate (EC), ethyl methyl carbonate (EMC), and dimethyl carbonate (DMC) containing lithium hexafluorophosphate ($LiPF_6$).

Charge–discharge cycle tests were performed at 25 and 60 °C with two ΔDOD conditions (0–100% and 10–70%). The charge–discharge cycle tests were operated at a current rate of 1 C (400 mA) in the voltage range of 4.2–2.5 V as 0–100% DOD and 4.05–3.48 V as 10–70% DOD.

Capacity checking test was inserted at every 50 cycles during the initial 500 cycles and at every 500 cycles during 500–2500 cycles to compare discharge capacity in the voltage region of 4.2–2.5 V among four conditions.

2.2. Deterioration analysis using coin-type model cells

In order to investigate the capacity deteriorations for the cathode and anode, cylindrical cells were disassembled to take out the cathode and anode, and each was rinsed by DMC, and then used to assemble a coin-type cell with a Li metal as a counter electrode under dry air atmosphere. The deterioration capacity was measured by charge–discharge tests and compared with a fresh electrode.

2.3. Surface and bulk analyses

Surface structure of each cathode was observed by XPS and scanning transmission microscopy (STEM)-EELS. The XPS analysis was performed with a Perkin–Elmer PHI 560/ESCA-SAM system. XPS spectra were obtained after several times of Ar^+-sputtering with 4 keV energy ions and a current beam of 0.36 μA cm^{-2}. A sample for the XPS analysis was excited with 1486.6 eV energy AlKα X-rays. STEM-EELS analysis was conducted with a 200 kV JEM-2100F equipped with a parallel electron energy loss (EEL) spectrometer (Gatan 863). XRD and SEM were used to study the phase change and microscopic morphology for active materials after cycling. For surface and bulk analyses, each cell was discharged to a voltage of 2.5 V at 1 C rate and then disassembled. The samples taken out of the disassembled cells were washed with dry DMC and evaporated at room temperature. Other experimental conditions are given in the next section.

3. Results and discussion

3.1. Cycle performance of cylindrical model cells after cycle tests in the controlled ΔDODs and cross-sectional SEM images of the NCA cathode

Fig. 1 shows charge–discharge cycle performance at 25 and 60 °C in two ΔDOD conditions for NCA cathode/graphite model cylindrical cells and the cross-sectional SEM images of the NCA cathode after cycle tests. The vertical axis or relative capacity is defined as the ratio of discharge capacity at a certain cycle to the initial one. In the ΔDOD condition of 0–100%, significant capacity fading and the growth of micro-cracks were observed, and the capacity deterioration was faster at higher temperature. On the

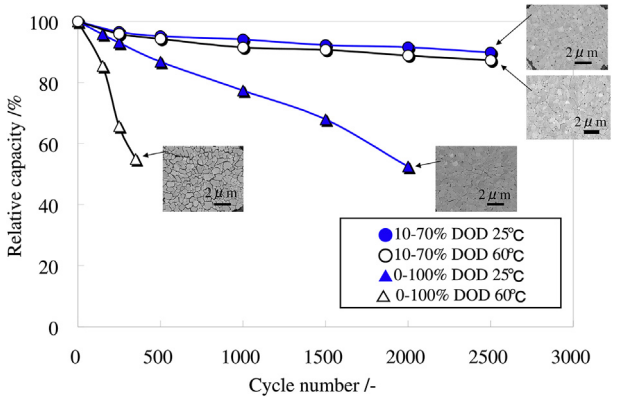

Fig. 1. Cycle performance of cylindrical model cells and cross-sectional SEM images of the NCA cathode in two ΔDOD conditions at 25 and 60 °C; (●) 10–70% at 25 °C, (○) 10–70% at 60 °C, (▲) 0–100% at 25 °C and (△) 0–100% at 60 °C.

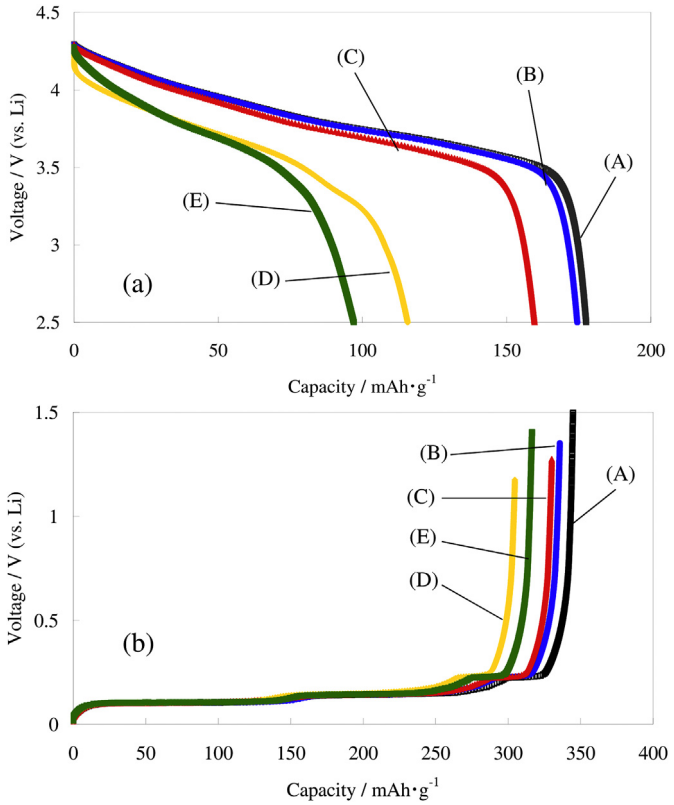

Fig. 2. Discharge curves of the cells with (a) NCA cathode electrode and (b) graphite anode electrode before and after cycle tests. Each curve was obtained from (A) a fresh cell and cycled cells with the conditions of (B) 10–70% DOD 25 °C, 2500 cycles, (C) 10–70% DOD 60 °C, 2500 cycles, (D) 0–100% DOD at 25 °C, 2000 cycles and (E) 0–100% DOD 60 °C, 350 cycles.

other hand, in the ΔDOD condition of 10–70%, cycle performance was greatly improved even at 60 °C, and micro-cracks were scarcely observed.

3.2. Characteristics of cathodes and anodes taken from cylindrical model cells after cycle tests in the controlled ΔDODs

The NCA cathode or graphite anode after cycle tests was reassembled into 2016 type coin cells with Li metal as a counter electrode. Fig. 2 shows discharge curves of the reassembled coin-type cells operated in a voltage region of 4.3–2.5 V for NCA cathode or of 1.0–0.01 V for graphite anode at a constant current of 0.1 C at 25 and 60 °C. After cycle tests in the ΔDOD of 0–100%, capacity loss for the cell with the NCA cathode was 33.5% at 25 °C and 45.2% at 60 °C, while that for the cell with the graphite anode was about 10%. These results suggest that the capacity loss is mainly ascribed to the deterioration of the NCA cathode which is influenced by ΔDOD and temperature. On the other hand, after cycle tests in the ΔDOD of 10–70%, capacity loss for the cell with the NCA cathode was 1.5% at 25 °C and 9.9% at 60 °C, These results indicate that the capacity loss is strongly affected by ΔDOD and test temperature.

3.3. Surface and cross section analysis of NCA cathode

In the macro structure analysis by XRD, there was not a large change between NCA cathodes before and after cycle tests irrespective of ΔDOD and temperature [2]. For surface and cross-sectional analyses by high-angle annular dark-field scanning transmission electron microscopy (HAADF-STEM), an NCA cathode was disassembled from a completely discharged cell and then washed with dry DMC and evaporated at room temperature. After that, the cathode was sliced by focused ion beam (FIB) method.

Fig. 3 shows the high-angle annular dark-field scanning transmission electron microscopy (HAADF-STEM) images and maps of C and F atoms for an NCA particle after 350 cycles in the ΔDOD of 0–100% at 60 °C. The C and F atoms which were ascribed to electrolyte mainly distributed in the micro-cracks of an NCA secondary particle. This suggests that the electrolyte infiltrated into the NCA particle through the micro-cracks. New SEI films are surely formed on the primary particle surface of NCA along the micro-cracks and the ionic/electric conductivity of the NCA particle would become worse remarkably.

Fig. 4 indicates C1s, O1s, F1s, Li1s and P2p core level spectra of NCA cathode before and after cycle tests of 350 cycles in the ΔDOD of 0–100% at 60 °C. There was no obvious change between spectra before and after cycle test for all elements although there was a little change in the O1s spectrum at the surface. The O1s spectrum after the cycle test was deconvoluted to that of $ROCO_2Li$, Li_2CO_3 and NCA ($LiMO_2$) as shown in Fig. 5. The $ROCO_2Li$ and Li_2CO_3 are included in an SEI film formed by electrolyte decomposition. The relative peak intensity of $ROCO_2Li$ or Li_2CO_3 to NCA ($LiMO_2$) (*I*ROCOOLi/*I*NCA ($LiMO_2$) or *I*Li_2CO_3/*I*NCA ($LiMO_2$)) before and after cycle tests in various conditions are summarized in Fig. 6. The relative peak intensity of $ROCO_2Li$, which was an oxidation product of electrolyte decomposition materials, after cycle tests at 60 °C became high, while that of Li_2CO_3 was relatively similar regardless of the condition of cycle test. The mechanism of the electrolyte decomposition reaction is proposed as follows [13–15].

$$EC + e^- \rightarrow EC^- \text{ (radical anion)} \quad (1)$$

$$2EC^- \text{ (radical anion)} \rightarrow \text{ethylene} + CH_2(OCO_2)^- \; CH_2(OCO_2)^- \quad (2)$$

$$CH_2(OCO_2)^- \; CH_2(OCO_2)^- + 2Li^+ \rightarrow CH_2(OCO_2Li) \; CH_2(OCO_2Li)(s) \quad (3)$$

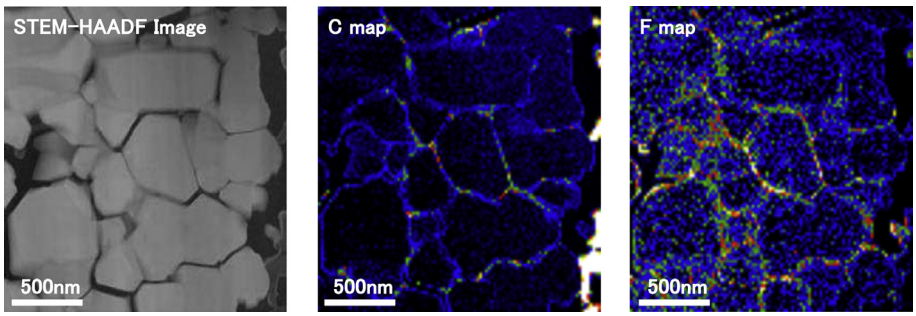

Fig. 3. HAADF-STEM images and maps of C and F atoms for an NCA particle after 350 cycles in the ΔDOD of 0–100% at 60 °C.

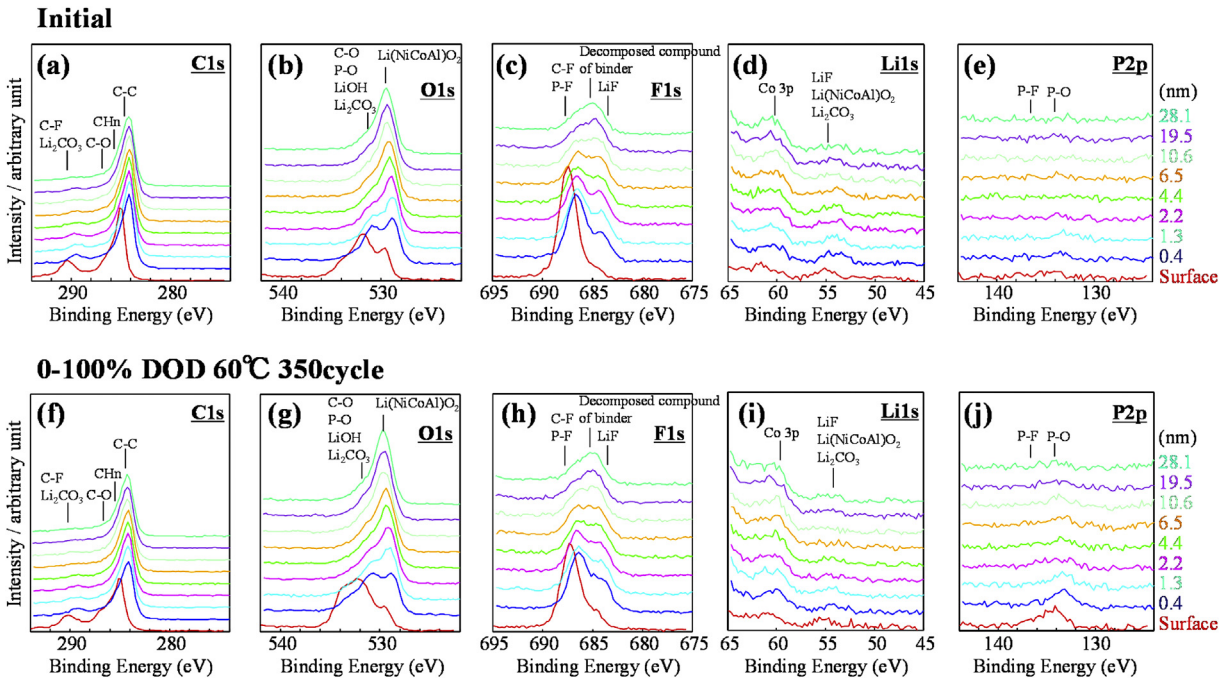

Fig. 4. (a, f) C1s, (b, g) O1s, (c, h) F1s, (d, i) Li1s and (e, j) P2p core level spectra of NCA cathode (a–e) before and (f–j) after cycle tests of 350 cycles in the ΔDOD of 0–100% at 60 °C. The numerical values in each figure indicate the distance from the surface.

$$DMC(CH_3OCO_2CH_3) + e^- + Li^+ \rightarrow CH_3OCO_2Li + CH_3^{\bullet} \quad (4)$$

$$EMC\ (CH_3CH_2OCO_2CH_3) + e^- + Li^+ \rightarrow CH_3CH_2OCO_2Li + CH_3^{\bullet} \quad (5)$$

or

$$EMC\ (CH_3CH_2OCO_2CH_3) + e^- + Li^+ \rightarrow CH_3OCO_2Li + CH_3CH_2^{\bullet} \quad (6)$$

CH_3or CH_3CH_2radical were converted to ether (CH_3OCH_3, $CH_3CH_2OCH_3$ and, $CH_3CH_2OCH_2CH_3$) and alkyl carbonate ($CH_3OCO_2CH_3$, $CH_3CH_2OCO_2CH_3$ and $CH_3CH_2OCO_2CH_2CH_3$).

Depth analysis of the O1s peak after the cycle test (Fig. 4(g)) exhibited the thickness of $ROCO_2Li$ film was about 4 nm. The relative peak intensity of $ROCO_2Li$ for the condition of 0–100% ΔDOD, 60 °C and 350 cycles which showed the largest capacity loss was smaller than that for the condition of 10–70% ΔDOD, 60 °C, 2500 cycles, indicating that the generation of $ROCO_2Li$ was not a dominant factor of deterioration. The relative peak intensity of $ROCO_2Li$ depended on test temperature and the elapsed time. The growth of SEI film was also affected by temperature and the elapsed

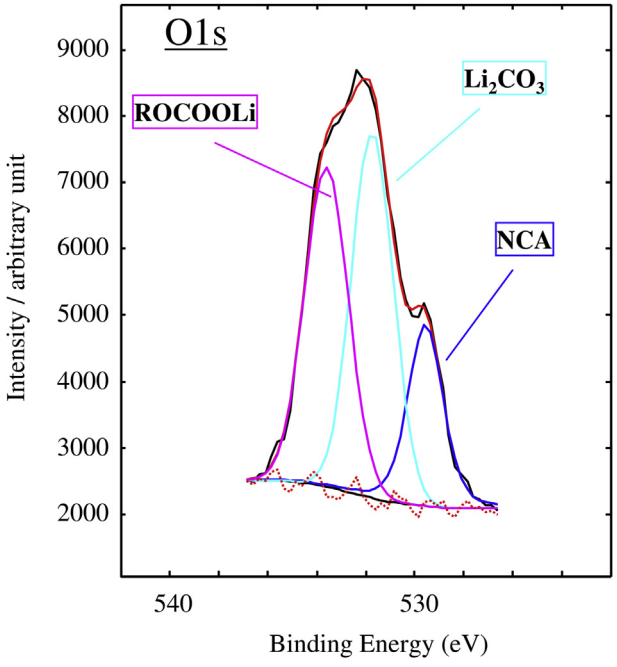

Fig. 5. O1s core level spectrum of NCA cathode after 350 cycles in the ΔDOD of 0–100% at 60 °C, $ROCO_2Li$, Li_2CO_3 and NCA ($LiMO_2$).

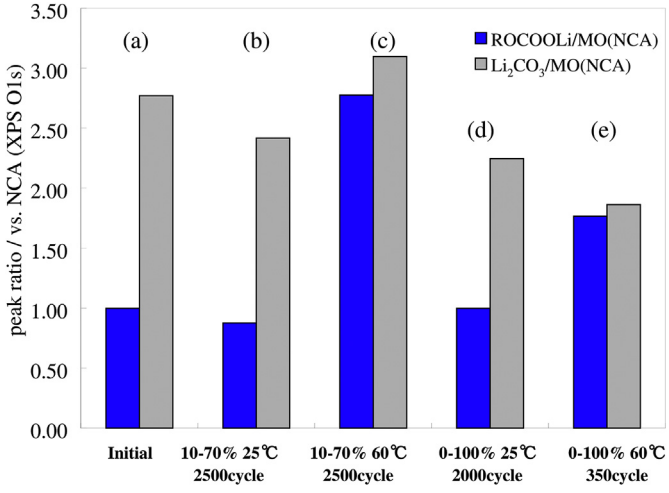

Fig. 6. Ratios of peak intensity of $ROCO_2Li$ or Li_2CO_3 to NCA ($LiMO_2$) in O1s core level spectra before and after cycle tests in various conditions. (a) before cycle test, (b) 10–70% ΔDOD, 25 °C, 2500 cycles, (c) 10–70% ΔDOD, 60 °C, 2500 cycles, (d) 0–100% ΔDOD, 25 °C, 2000 cycles and (e) 0–100% ΔDOD, 60 °C, 350 cycles.

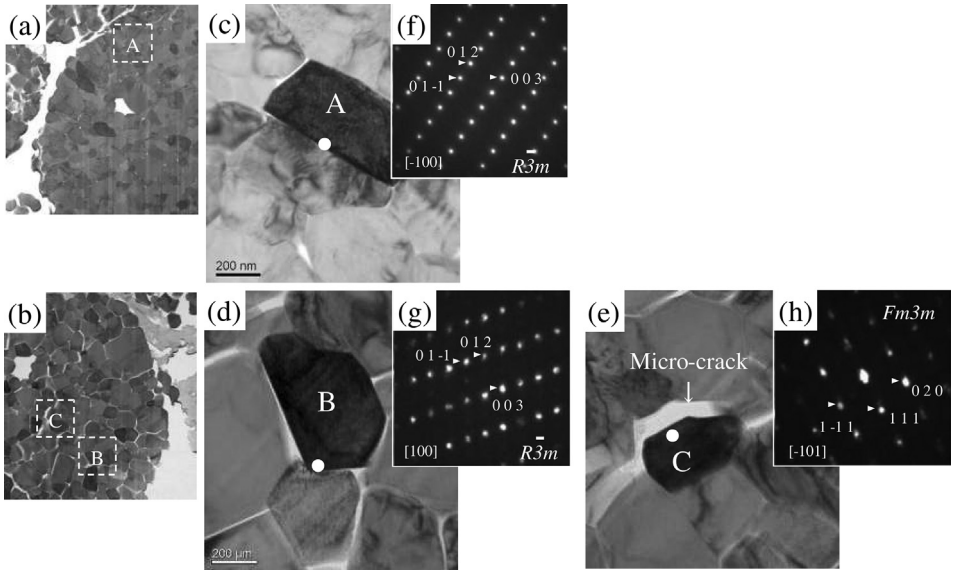

Fig. 7. Cross-sectional TEM images (a, b), their magnifications (c–e) and corresponding SAED patterns (f–h) of NCA cathodes before (a, c, f) and after (b, d, e, g, h) cycle tests in the ΔDOD of 0–100%. SAED patterns (f, g) were obtained from edge (A and B) of a primary particle faced on the neighbor particle, while SAED pattern (h) was obtained from that (C) faced on micro-crack.

time, but the SEI film with about several nanometers in thickness did not influence any electrochemical performance.

The contact of fresh NCA surface with new electrolyte due to the growth of micro-cracks led to deterioration in battery performance. Therefore we investigated the change of the interface in the grain boundary of NCA by TEM and EELS analysis.

Fig. 7 shows TEM images and the corresponding selected area electron diffraction (SAED) patterns of NCA particles before and

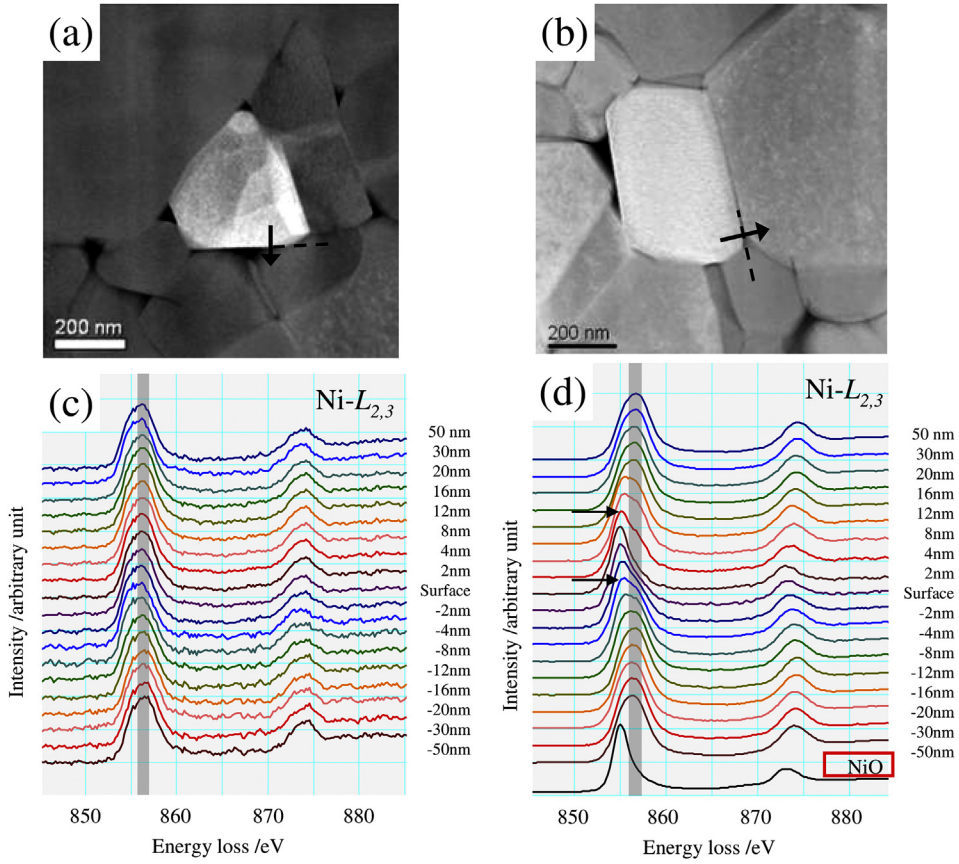

Fig. 8. STEM-ADF images (a, b) and Ni-*L* edge EELS spectra (c, d) for the surface of a primary particle of NCA cathode. (a, c) Before and (b, d) after immersion and then first charge–discharge cycle.

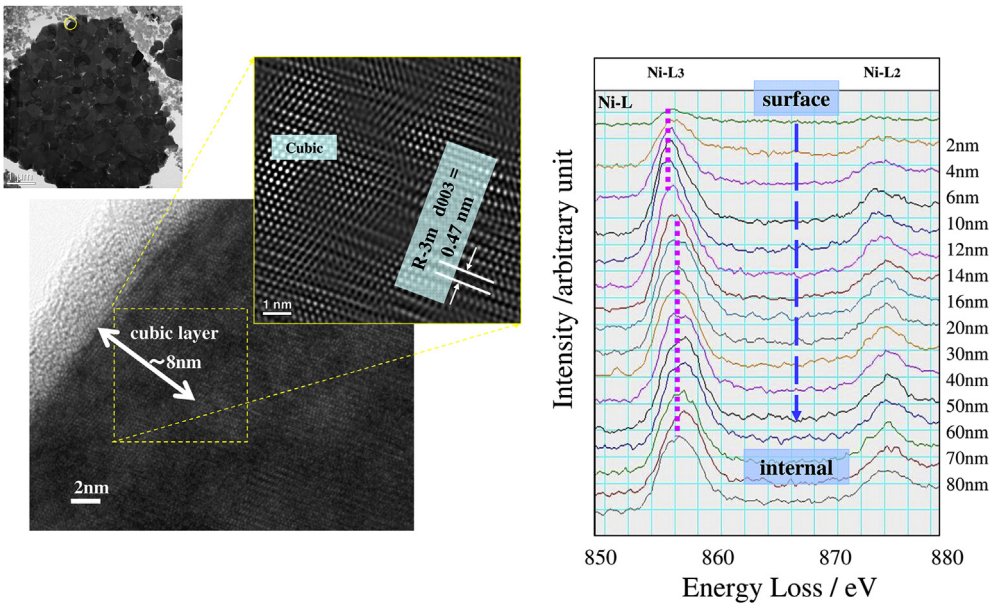

Fig. 9. Cross-sectional TEM images and depth profiles of STEM-EELS for NCA surface after cycle test of 5000 cycles in the ΔDOD of 10–70% at 25 °C.

after cycle tests of 350 cycles in the ΔDOD of 0–100% at 60 °C. Before the cycle test, there were no cracks in NCA particles and the electron diffraction pattern (Fig. 7(f)) exhibited that the surface of a primary particle had R3m crystal structure. On the other hand, after the cycle test, many cracks were observed in a secondary particle. The R3m structure was maintained at the surface of a primary particle faced on neighbor one (Fig. 7(g)), but a Fm3m rock salt like structure was formed at a primary particle faced on micro-crack (Fig. 7(h)). This seems to be a NiO-like layer, as reported previously [6,7,11,12]. NiO is known to have poor conductivities of lithium ions and electrons, so the resistance layer formed inside secondary particles would contribute to the rise in impedance.

In order to examine why the resistance layer was formed only at vicinity of micro-cracks, STEM-EELS analyses were performed. Fig. 8 shows STEM-ADF images and Ni-*L* edge EELS spectra for the surface of a primary particle of NCA cathode before immersion to electrolyte and after immersion and then the first charge–discharge cycle. Before immersion, no peak shift was observed in the EELS spectra (Fig. 8(c)). However, after immersion and the first charge–discharge cycle, a peak shift in the low energy direction was detected at around 4 nm in depth from the primary particle surface (shown by arrows in Fig. 8(d)). The shifted peak position was identical to that of NiO as shown in Fig. 8(d), suggesting that the NiO-like layer was formed at the interface between electrolyte and NCA particles during the first charge–discharge cycle. These results are agreement with the recent investigation by Ukyo et al. [11,12]. From these results, the micro-crack generation would be accompanied by penetration of electrolyte into NCA secondary particles to form a new NiO-like layer.

Figs. 9 and 10 show cross-sectional TEM images and depth profiles of Ni-*L* edge EELS spectra for the NCA particle surface after 5000 cycles in the ΔDOD of 10–70% at 25 and 60 °C. No micro-

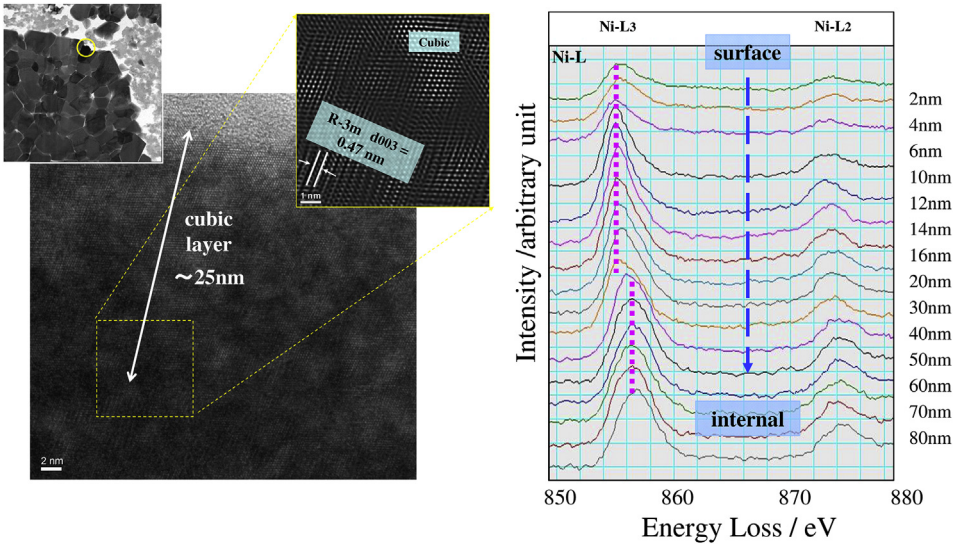

Fig. 10. Cross-sectional TEM images and depth profiles of STEM-EELS for NCA surface after cycle test of 5000 cycles in the ΔDOD of 10–70% at 60 °C.

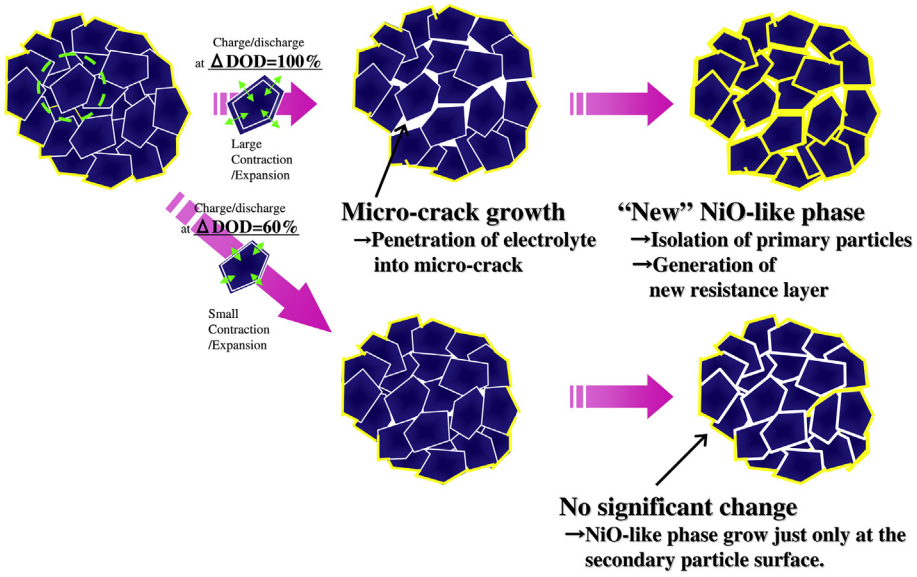

Fig. 11. A schematic model for the deterioration of NCA particle during cycle test.

cracks evolved even after 5000 cycles at both temperatures. The generation rate of NiO-like layer was increased with increasing the cycle test temperature. The thickness of NiO-like layer was increased to 8 nm at 25 °C and 25 nm at 60 °C. Therefore, the growth of NiO-like layer on the secondary particle surface can be suppressed even after 5000 cycles at 60 °C as long as ΔDOD is restricted to 10–70%.

On the other hand, the NiO-like layer was formed on most of the primary particle surface after charge–discharge cycling in the ΔDOD condition of 0–100%. So the infiltration of electrolyte can cause the formation of surface film and the NiO-like interface layer. Lack of contact between primary particles and the increase in resistance layer are caused by micro-crack generation, which leads to capacity fading and impedance increase. It is important to suppress the micro-crack generation to achieve excellent cycle life.

A schematic model for the deterioration of NCA particle during cycle test is shown in Fig. 11. For the cycle test in the ΔDOD of 0–100%, micro-cracks easily generate in the secondary particles because of the stress with shrinkage and expansion of NCA crystal lattices is larger compared with the cycle test in the restricted ΔDOD. The electrolyte infiltrates into the micro-cracks and causes the formation of the surface SEI film and the NiO-like interface layer. The NiO-like layer with the rock salt-type crystal structure shows low lithium ion conductivity and low electric conductivity, which would cause lack of electric contact between the primary particles and the inhibition of lithium ion transport into the surface layer. Consequently, this leads to capacity fading and rise in impedance. At higher operation temperatures, the formation rate of the NiO-like layer in micro-crack regions is increased and the deterioration of the cell capacity is accelerated. In contrast, for the cycle test in the ΔDOD of 10–70%, the generation of micro-cracks is effectively prevented and the formation of NiO-like layer is also limited near the surface of the secondary particle surface, not the primary particle surface.

4. Conclusion

The mechanism of cycle life deterioration for LIBs with the NCA cathode was investigated by analyzing the Li $Al_{0.10}Ni_{0.76}Co_{0.14}O_2$ cathode after cycle tests in different ΔDOD conditions using some spectroscopic methods such as XPS, HAADF-STEM and STEM-EELS. The following findings were obtained.

(1) The residual capacity depended on ΔDOD and temperature. When ΔDOD was restricted to 10–70%, cycle life at 25 °C was maintained even at 60 °C, while the generation and growth of micro-cracks were often observed especially at 60 °C as the ΔDOD was 0–100% (4.2 V–2.5 V).
(2) The growth of SEI film on the NCA surface was hardly detected by XPS.
(3) The electrolyte infiltrated into the NCA secondary particles with the generation of micro-cracks, and the NiO-like structure layer was formed on the primary particle surfaces, causing the rise in impedance.
(4) The formation rate of the NiO-like layer was accelerated in the cycle test at 60 °C and the impedance rise was further accelerated.
(5) The micro-crack generation and the growth of the NiO-like structure layer on the primary particle surface were the main reason of the NCA cathode deterioration.

Acknowledgments

This work was supported by the "Li-EAD"program of the New Energy and Industrial Technology Development Organization (NEDO). The authors express their thanks to members of Lithium ion Battery Business Unit (A. Nagasaki, N. Yamamoto and H. Kaiya) and Prof. Hiroshi Inoue in Osaka Prefecture University.

References

[1] S. Watanabe, M. Kinoshita, K. Nakura, J. Power Sources 196 (2011) 6906.
[2] S. Watanabe, T. Hosokawa, K. Morigaki, M. Kinoshita, K. Nakura, ECS Trans. 41 (2012) 65.
[3] A.M. Andersson, D.P. Abraham, R. Haasch, S. MacLaren, J. Liu, K. Amine, J. Electrochem. Soc. 149 (2002) A1358.
[4] D.P. Abraham, J. Liu, C.H. Chen, Y.E. Hyung, M. Stoll, N. Elsen, S. MacLaren, R. Twesten, R. Haasch, E. Sammann, I. Petrov, K. Amine, G. Henriksen, J. Power Sources 119 (2003) 511.
[5] R. Kostecki, J. Lei, F. McLarnon, J. Shim, K. Striebel, J. Electrochem. Soc. 153 (2006) A669.
[6] D.P. Abraham, R.D. Twesten, M. Balasubramanian, I. Petrov, J. McBreen, K. Amine, Electrochem. Commun. 4 (2002) 620.
[7] D.P. Abraham, R.D. Twesten, M. Balasubramanian, J. Kropf, D. Fischer, J. McBreen, I. Petrov, K. Amine, J. Electrochem. Soc. 150 (2003) A1450.
[8] H. Kobayashi, M. Shikano, S. Koike, H. Sakaebe, K. Tatsumi, J. Power Sources 174 (2007) 380.

[9] M. Shikano, H. Kobayashi, S. Koike, H. Sakaebe, E. Ikenaga, K. Kobayashi, K. Tatsumi, J. Power Sources 174 (2007) 795.
[10] D. Mori, H. Kobayashi, M. Shikano, H. Nitani, H. Kageyama, S. Koike, H. Sakaebe, K. Tatsumi, J. Power Sources 189 (2009) 676.
[11] S. Zheng, R. Huang, Y. Makimura, Y. Ukyo, C.A.J. Fisher, T. Hirayama, Y. Ikuhara, J. Electrochem. Soc. 158 (2011) A357.
[12] Y. Makimura, S. Zheng, Y. Ikuhara, Y. Ukyo, J. Electrochem. Soc. 159 (2012) A1070.
[13] D. Aurbach, Y. Ein-Eli, O. Chusid, Y. Carmeli, M. Babai, H. Yamin, J. Electrochem. Soc. 141 (1994) 603.
[14] D. Aurbach, B. Markovsky, A. Shechter, Y. Ein-Eli, J. Electrochem. Soc. 143 (1996) 3809.
[15] P. Arora, R.E. White, M. Doyle, J. Electrochem. Soc. 145 (1998) 3647.